The Effects of Colloidal Nanotopography on Initial Fibroblast Adhesion and Morphology

Mairead A. Wood* , Chris D. W. Wilkinson, and Adam S. G. Curtis

***Abstract*—Colloidal lithography offers a simple, inexpensive method of producing irregular nanotopographies, a pattern not easily attainable utilizing conventional serial writing processes. Colloids with 20- or 50-nm diameter were utilized to produce such an irregular topography and were characterized by calculating the percentage area coverage of particles. Interparticle and nearest neighbor spacing were also assessed for the individual colloids in the pattern. Two-way analysis of variance (ANOVA) indicated significant differences between the number of fibroblasts adhering to planar, 20-, and 50-nm-diameter colloidal topographies, the number of fibroblasts adhering to the substrates at the time intervals studied, namely 20 min, 1 h, and 3 h and significant interaction between time and topography on fibroblast adhesion ($P < 0.01$). Tukey tests were utilized for sensitive identification of the differences between the sample means and compounded ANOVA results. Cytoskeletal and general cell morphology were investigated on planar and colloidal substrates, and indicated cells in contact with irregular nanotopographies exhibit many peripheral protrusions while such protrusions are absent in cells on planar control surfaces. These protrusions are rich in microtubules on 20-nm-diameter colloidal surfaces while microfilaments are prevalent on 50-nm-diameter surfaces. Moreover, by 3 h, cells on the colloidal substrates initiate cell–cell adhesions, also absent in controls.**

***Index Terms*—Actin and tubulin cytoskeleton, cell adhesion and morphology, colloidal lithography, fibroblasts, nanotopography.**

I. Introduction

THE EFFECTS OF cell–substrate adhesions are directly linked to fundamental cell behaviors, for example, cell polarization, spreading, and motility [1], [2]. Such processes are necessary for proliferation, ultimately determine cell-cycle progression, and are dependent on the nature of adhesions established by the cell, the interactions of adhesions with the cytoskeleton via focal adhesion complex (FAC)-associated proteins and thus signal transduction and gene regulation [3]–[6]. Bidirectional signaling and interfacing between the cell cytoskeleton and integrins is crucial for cell response to a given substrate [7]. Thus, cell reactions can be managed by controlling the characteristics of a surface, for example, topography, chemistry, and viscoelastic properties [8], although it should be noted these are likely to work in a synergistic manner [9].

Fibroblasts have a pivotal role during the initial phases of implant integration and resultant healing processes [10], [11]. Materials must fit criteria specific to the tissue under reconstruction including the mechanical properties, chemistry, and physical architecture of an implant relative to the native tissue where it will be situated. With respect to the tissue–implant interface, *in vitro* investigations indicate that microtopography can be utilized to control cell behavior, including that of fibroblasts, via initial adhesive interactions [12]–[15]. Furthermore, the effects of nanopatterned surfaces on cell adhesion and behavior have emerged in-line with developments in electronics and materials fabrication techniques [16]–[23], compounding the importance of substrate topography on micro- and nanometric levels in fundamental cell behavior [24], [25].

Development of nanofabrication techniques has enabled the production of a variety of nanotopographies for biological research, allowing for the elucidation of nanofeature effects on cell behavior [26]–[29]. Investigations into cell response to nanotopographies require surfaces patterned over large areas in batch, which are highly reproducible, high throughput, preferably inexpensive and fabricated in biocompatible materials. As a result, in-plane nanopatterning of substrates applied to date in biological investigations have utilized a number of fabrication techniques fitting this criteria, including conventional photolithography techniques [30] and reactive ion etching (RIE) [31], colloidal-based lithography [19], [20], replication technologies [32], and polymer demixing techniques [21].

Nanoparticles offer suitably sized, functional components for developing in-plane patterns [33]. Natural lithography [34], [35], is an extremely convenient route to developing nanofeatures over large areas for biological investigations. Colloidal gold particles, previously utilized in the development of single-electron devices [36], have emerged as a versatile method of producing nanometric features [37]. Every aspect of nanopatterning can be altered with respect to colloidal fabrication techniques, for example, colloidal and substrate materials, colloidal shape, size, and monolayer distribution which is reflected in feature pitch [33]. Furthermore, electrostatic repulsion occurring between individual colloids results in irregular monolayer patterning in the absence of charge shielding materials. Irregular patterning of substrates utilizing alternative nanofabrication techniques, for example, e-beam

Manuscript received April 19, 2005; revised September 8, 2005. This work was supported in part by the EPSRC under EU framework V grant QLK 3-CT-2000-01500 (Nanomed) and in part by the EU Framework V Growth Programme under Grant GRD5-CT2000-00375 (Magnanomed). *Asterisk indicates corresponding author.*

*M. A. Wood is with the Division of Infection and Immunity, Centre for Cell Engineering, University of Glasgow, Glasgow G12 8QQ, U.K. (e-mail: m.wood@bio.gla.ac.uk).

C. D. W. Wilkinson is with the Department of Electrical Engineering, University of Glasgow, Glasgow G12 8QQ, U.K..

A. S. G. Curtis is with the University of Glasgow, Glasgow G12 8QQ, U.K. (e-mail: a.curtis@bio.gla.ac.uk).

Digital Object Identifier 10.1109/TNB.2005.864015

lithography, is time consuming and difficult; thus, colloidal lithography is greatly advantageous for irregular in-plane nanopattern production.

Biological studies into the effects of topographical cues, both at the micro- and nanometric levels, have revealed that feature dimensions are paramount to elicited cellular response, where adjustments in a single plane can often have a dramatic effect on cell behavior. Thus, biological strategies utilizing controlled topographies offer methods of optimizing implant integration and furthering our understanding of fundamental cell behavior in response to specific substrate patterns. In this paper, colloidal lithography was used to fabricate irregular nanotopographies with features of either 20- or 50-nm diameter. Colloids were adhered to a silica base substrate via an aminosilane, and interparticle spacing was determined by electrostatic repulsion occurring between individual particles. Colloidal surfaces were characterized by calculating percentage area coverage of colloids in relation to the base substrate and interparticle spacing reflecting feature pitch. The effect of time and topography on fibroblast adhesion was investigated, and cell morphology and behavior in relation to the colloidal topographies are discussed.

II. Materials and Methods

A. Fabricating Colloidal Nanotopographies

Silicon or glass base substrates with silica (SiO_2) surface were prepared as described elsewhere [19]. Briefly, an active silanol was created by adding a solution of 200 μL of 0.1% N-(β-Aminoethyl)-Ψ-amino-propyltrimethoxysilane (AAPS) (Pierce Biotechnology Inc., Rockford, IL, product no. 80379) dissolved in 9.8 ml of acetic ethanol to the silica surface for 20 min using a syringe with 0.2-μm dosing filter. Substrates were then washed in 100% ethanol and rinsed with RO water under sonication. Subsequently, substrates were immersed in either a 20- or 50-nm-diameter colloidal sol (product nos. EM.GC20 and EM.G50, respectively, British Biocell International Ltd, Cardiff, U.K.), depending upon the size of nanofeature being sought, six times at 15-min intervals. Structures were removed from the sol following this period and left to dry naturally, with the remaining solution evaporating from the surface over time resulting in a submonolayer, irregular colloidal nanotopography.

B. Characterization of Colloidal Nanotopographies

Following fabrication to the nanotopographies, images captured using a Hitachi S-900 (detailed below) were used to calculate percentage area coverage of colloids in relation to the silica base substrates and interparticle spacing. Using the scale bar in each image, 500 nm in relation to the 20-nm-diameter colloids and 1 μm with respect to the 50-nm-diameter colloids (Fig. 1(a) and (b), respectively), a square with sides equal to the scale bar was measured onto an acetate sheet and placed over the micrograph in question. The image was printed at A4-size, allowing for more accurate measurements to be obtained. The width and height proportions for all images used were constrained using this option available in Adobe Photoshop, preventing corruption of the original dimensions. The number of colloids contained within 12 nonspecifically selected areas were counted and used

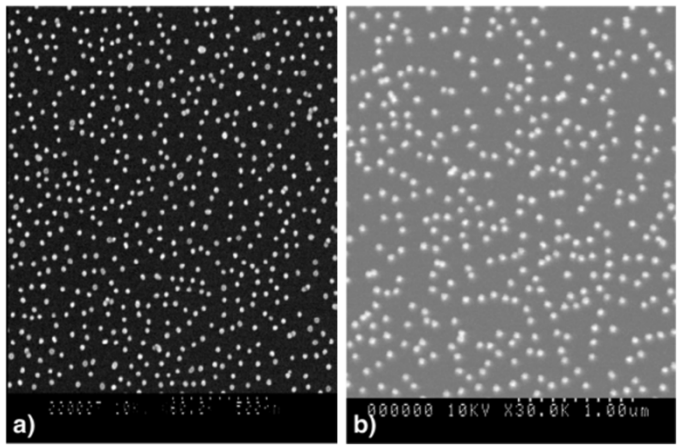

Fig. 1. Scanning electron microscgraph captured using the Hitachi S-900 FESEM of: (a) 20-nm-diameter colloids (x60K, scale bar $=$ 500 nm) and (b) 50-nm-diameter colloids (x30K, scale bar $=$ 1 μm). These images were used to calculate percentage area coverage and interparticle spacing of the colloids composing the nanotopographies in relation to their silica base substrate.

to calculate percentage area coverage of the particles relative to the base substrate. The three nearest neighbor distances for each individual particle within the given area was then calculated using center-to-center measurements. These methods are described in further detail elsewhere [38].

C. Cell Culture Techniques

hTERT BJ-1 Infinity Telomerase-Immortalized human fibroblasts (Clontech Laboratories, Inc.) were seeded onto the nanotopographies at a volume of 10 000 cells per ml in 3 ml and cultured in complete Dulbecco's modified eagle's medium (DMEM) (70% DMEM, 18% Medium 199, 9% fetal bovine serum (FBS), 2% antibiotics and 1% 100 mM sodium pyruvate). Samples were incubated at 37 °C and CO_2 buffered.

D. Fibroblast Adhesion Assay

Following culture on the nanotopography for either 20 min, 1 h, or 3 h, media was removed and samples were rinsed in phosphate buffered saline (PBS) with gentle agitation to ensure removal of nonattached cells and fixed in formalin (4% formaldehyde in PBS) for approximately 10 min at 37 °C. Coomasie blue solution was used as a nonspecific protein stain, highlighting cell nuclei and morphology allowing for their easier identification on the substrates. Fibroblast adhesion on each experimental surface was measured by first counting 30 nonspecifically chosen fields of view measuring 0.93×0.93 mm^2 using a Vickers light microscope with 10× Phaco 1 objective lens (170/-, 10/0.25). One nucleus was counted as one cell.

E. Preparation of Samples for Use With Field Emission Scanning Electron Microscope (FESEM)

Following culture on the colloidal nanotopographies, samples to be imaged using a Hitachi S-900 FESEM were rinsed twice in PBS. Cells were then fixed in 2.5% gluteraldehyde suspended in 0.1 M phosphate buffer (MPO_4) for 30 min. Three changes of 0.1 PO_4 buffer at 10-min intervals follows to ensure complete removal of excess gluteraldehyde. A 1% osmium tetroxide (OSO_4) solution was then reacted with the samples for 30 min

to maximize contrast between the cell and the surrounding substrate. Samples were subsequently rinsed three times in distilled water at 10-min intervals. An alcohol dehydration series (30%, 40%, 50% 60%, 70%, 80%, 90%, and 96%) with each step lasting for 10 min followed with samples being rinsed twice in absolute alcohol (100% ethanol) for 10 min and then dried absolute alcohol for a further 10 min. Samples were placed in porous sample holders and critically point dried for approximately 1 h 40 min with ethanol as the dehydrant and liquid CO_2 as the transitional fluid. Samples containing cells were sputter coated with 10 nm gold–palladium (Au/Pd, 80/20) using an Emscope SC 500 (Emtech Ltd, Kent, U.K.) sputter coater prior to viewing on the Hitachi S-900. Samples housing the colloidal nanotopography were not coated prior to SEM imaging. Images were captured and processed using Quartz PCI (Quartz Imaging Corp., Vancouver, BC, Canada) imaging program.

F. Fluorescent Staining and Imaging of F-Actin and Tubulin Cytoskeleton

Following culture, cells were washed and permeabilized on their given substrate before adding β-tubulin primary antibody raised in mouse anti-human and an F-actin probe, rhodamine Phalloidin diluted 1 : 50 in 1% BSA/PBS. Samples were incubated in the solution for 1 h at 37 °C and then rinsed in 0.5% Tween 20/PBS at room temperature before adding the secondary antibody for tubulin (biotinylated horse anti-mouse) 1:50 in 1%BSA/PBS for 1 h at 37 °C. Structures were then washed in 0.5% Tween20/PBS at room temperature, and fluorescein-streptavidin, 1:50 with 1%BSA/PBS, which binds biotin, was added to the samples for 30 min at 4 °C. Samples were then washed in 0.5% Tween20/PBS before being mounted on a glass microscope slide with Vectashield (containing Dapi, a DNA stain), and placing a glass coverslip on top of the sample. Fluorescent cells were then viewed in relation to the colloidal nanotopography using a Vickers M17 microscope in oil immersion mode with 50× objective.

G. Statistical Analysis

With respect to interparticle spacing used to characterize the colloidal nanotopographies, Microsoft Excel was used to calculate general descriptive statistics. The mean, standard deviation, standard error, minimum, and maximum distances between nearest neighboring colloids in the populations investigated, and the count (n), indicating the number of colloids used to calculate the smallest distance to their nearest neighbor was thus determined.

Data accumulated with respect to the number of fibroblasts adhering to 20-nm-diameter, 50-nm-diameter colloidal and control, planar substrates was entered into Statview (Abacus Concepts Inc.), a statistical analysis program. Descriptive statistics and distribution histograms were obtained for each surface at each time point and indicated data was normally distributed and variance was homogenous. A parametric two-way analysis of variance (ANOVA) was thus selected to analyze the influence of two independent variables, topography and time, upon fibroblast adhesion, and was conducted as described by Fowler *et al.* [39]. Following identification of statistically significant differences between the fibroblast adhesion sample means using ANOVA, a Tukey test was utilized to provide sensitive identification of differences between the means, and was calculated by constructing a Tukey trellis for two-way ANOVA [39].

TABLE I
CHARACTERIZATION OF COLLOIDAL NANOTOPOGRAPHIES, INCLUDING PERCENTAGE AREA COVERAGE AND NEAREST NEIGHBOR DESCRIPTIVE STATISTICS OF 20–NM-DIAMETER AND 50 NM-DIAMETER COLLOIDS ADHERED TO SILICA BASE SUBSTRATES FOLLOWING 24-H SOL IMMERSION

Colloidal Diameter	20nm	50nm
Percentage area coverage	5.13%	7.13%
Mean interparticle spacing	56.80nm	113.78nm
Standard Deviation	11.35nm	41.93nm
Standard Error	0.87nm	3.61nm
Count (n)	172	135
Minimum	20.00nm	50.00nm
Maximum	90.00nm	290.00nm

III. RESULTS

A. Percentage Area Coverage and Interparticle Spacing of Colloids Composing Nanotopographies

Scanning electron micrographs were captured of the 20-and 50-nm-diameter colloidal topographies (Fig. 1(a) and (b), respectively) and were used to calculate percentage area coverage in relation to the base substrate and interparticle spacing of colloids (Table I). Colloidal coverage was calculated at approximately 5% for aminosilanized substrates immersed in 20-nm-diameter colloidal sol six times at 15 min intervals and 7% for substrates immersed in the 50-nm-diameter colloidal sol. Immersion in the sols overnight (12–24 h) was later found to produce very similar colloidal coverage and interparticle spacing [40], suggesting submonolayer saturation is a time-dependent phenomenon [41]. Mean distance between nearest neighboring 20-nm-diameter colloids was 56.80 nm, where $n = 172$. Minimum distance between neighboring 20-nm-diameter colloids was 20 nm, indicating the occurrence of colloids in contact with one another. Maximum spacing between nearest neighbors for 20-nm-diameter colloids was 90 nm, and standard deviation and standard error were calculated as 11.35 and 0.87, respectively. With respect to substrates coated with 50-nm-diameter colloids, mean distance was calculated as 113.78 nm, where $n = 135$. The minimum distance between neighboring colloids, 50 nm, indicates that in some instances neighboring colloids were in contact with one another. A maximum distance of 290 nm was calculated between 50-nm-diameter neighboring colloids, and a standard error of 41.93. Standard error occurring in the one hundred thirty–five 50-nm-diameter colloids investigated was calculated as 3.61.

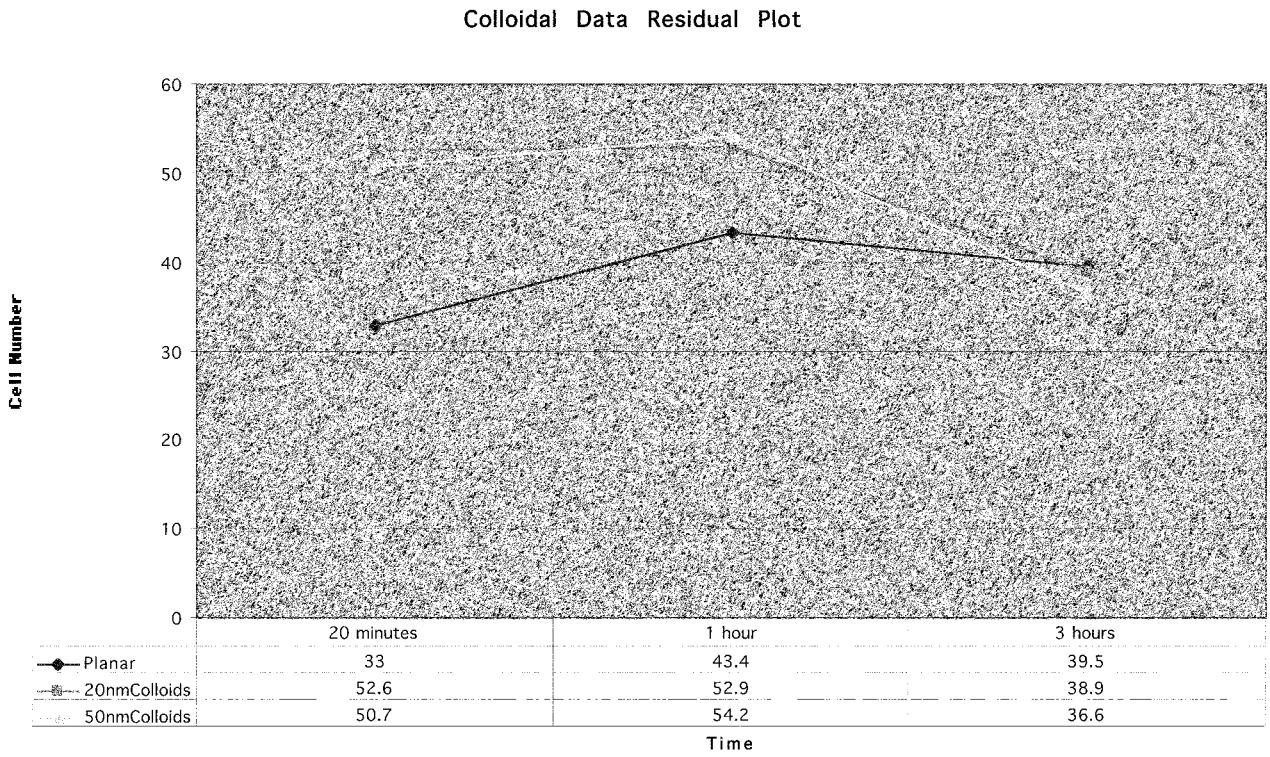

Graph 1. Residual plot of mean fibroblast adhesion on planar, 20-, and 50-nm-diameter colloidal topographies at 20 min, 1 h, and 3 h. Lines connecting the mean values, written in the table at the base of the graph, are not consistently parallel between the number of cells adhering on each substrate at each time interval, indicating possible interaction between the variables. Interaction is further supported at 3 h where lines connecting the means crossover one another or interact.

TABLE II
ANOVA TABLE SUMMARIZING FIBROBLAST ADHESION DATA. F-VALUES EXCEED THE CRITICAL VALUE AT $P = 0.01$ FOR THE APPROPRIATE NUMBERS OF DEGREES OF FREEDOM WHEN REFERRING TO A TABLE OF DISTRIBUTION OF F (FOWLER et al., 1998, APPENDIX 10).** INDICATES SIGNIFICANCE AT $p < 0.01$

Source of variation	Sum of squares	df (degrees of freedom)	Variance	F
(between samples)	(15628.34)	(8)		
Variable A Time	*6396.31*	*2*	*3198.16*	*9.84***
Variable B Topography	*4889.09*	*2*	*2444.55*	*7.52***
Interaction	4342.94	4	1085.74	*3.34***
Within samples	84873.23	261	325.18	

B. The Effects of Colloidal Nanotopographies on Fibroblast Adhesion

The mean number of fibroblasts adhering to each individual topography, namely control planar, 20-, and 50-nm-diameter colloidal surfaces, at each time point, 20 min, 1 h, and 3 h were used to form a residual plot (Graph 1). The residual plot of the means indicates that cell adhesion increases on all three substrates between 20 min and 1 h, and decreases between 1 and 3 h. However, the rates of increase and decrease at these periods are not equal, indicating a possible interaction between the variables, namely time and topography, on fibroblast adhesion. Two-way analysis of variance was used to identify the effects and interaction between the two independent variables, time and topography, in question (Table II).

The first null hypothesis states there are no significant differences between the number of fibroblasts adhering to planar, 20-, and 50-nm-diameter colloidal substrates (variable B). However, the value of $F = 7.52$ for variable B (Table II) exceeds the tabulated value at $P = 0.01$ where F-distribution is recorded as 4.6052 when degrees of freedom (df) $= 2, 261$. H_0 is thus rejected, indicating that surface topography affects fibroblast adhesion.

Similarly, the second null hypothesis states that there are no significant differences between time and the number of fibroblasts adhering to each individual substrate. The F value, 9.84, calculated using the original data for variable A (Table II) exceeds the tabulated value at $P = 0.01$ of 4.6052 for df 2, 261. The null hypothesis is thus rejected, concluding that the number of fibroblasts adhering to each individual substrate at the time

TABLE III
A TUKEY TRELLIS FOR TWO-WAY ANOVA WAS USED TO IDENTIFY DIFFERENCES BETWEEN SAMPLE MEANS OF FIBROBLAST ADHESION WITH RESPECT TO TOPOGRAPHY AND TIME, WHERE TEST STATISTIC $T = 14.45$. THERE ARE 9 OUT OF A POSSIBLE 36 PAIRS OF MEANS WHOSE DIFFERENCES EXCEED THIS VALUE AND WHOSE DIFFERENCES ARE STATISTICALLY SIGNIFICANT AT $P = 0.05$ (HIGHLIGHTED IN LIGHT FONT)

Sample	2 (20nm/ 20min)	3 (50nm/ 20min)	4 (planar/ 1hr)	5 (20nm/ 1hr)	6 (50nm/ 1hr)	7 (planar/ 3hrs)	8 (20nm/ 3hrs)	9 (50nm/ 3hrs)
Sample 1 (planar/20min) X=33	(X_1-X_2) 19.6	(X_1-X_3) 17.7	(X_1-X_4) 10.4	(X_1-X_5) 19.9	(X_1-X_6) 21.2	(X_1-X_7) 6.5	(X_1-X_8) 5.9	(X_1-X_9) 3.6
Sample 2 (20nm/20min) X=52.6		(X_2-X_3) 1.9	(X_2-X_4) 9.2	(X_2-X_5) 0.3	(X_2-X_6) 1.6	(X_2-X_7) 13.1	(X_2-X_8) 13.7	(X_2-X_9) 16
Sample 3 (50nm/20min) X=50.7			(X_3-X_4) 7.3	(X_3-X_5) 2.2	(X_3-X_6) 3.5	(X_3-X_7) 11.2	(X_3-X_8) 11.8	(X_3-X_9) 14.1
Sample 4 (planar/1hr) X=43.4				(X_4-X_5) 9.5	(X_4-X_6) 10.8	(X_4-X_7) 3.9	(X_4-X_8) 4.5	(X_4-X_9) 6.8
Sample 5 (20nm/1hr) X=52.9					(X_5-X_6) 1.3	(X_5-X_7) 13.4	(X_5-X_8) 14	(X_5-X_9) 16.3
Sample 6 (50nm/1hr) X=54.2						(X_6-X_7) 14.7	(X_6-X_8) 15.3	(X_6-X_9) 17.6
Sample 7 (planar/3hrs) X=39.5							(X_7-X_8) 0.6	(X_7-X_9) 2.9
Sample 8 (20nm/3hrs) X=38.9								(X_8-X_9) 2.3
Sample 9 (50nm/3hrs) X=36.6								

intervals investigated are significantly different, thus following initial cell seeding, fibroblast adhesion is significantly different at 20 min, 1 h, and 3 h with respect to the topographies investigated.

The third null hypothesis employed asserts there is no interaction between the substrate topography and time, which influences the mean number of fibroblasts adhering to a surface. The F value calculated for the interaction between variable A (time) and B (topography), 3.34, exceeds the tabulated value of $P = 0.01$, of approximately 3.3192 for df 4, 261, resulting in rejection of the null hypothesis. Thus, it can be concluded that an interactive effect between topography and time acts to influence fibroblast adhesion.

The results of the two-way analysis of variance indicate there are statistically significant differences between the means of the samples, however further analysis is required to identify the specific means that are statistically different. The Tukey Test allows for sensitive identification of differences between the means,

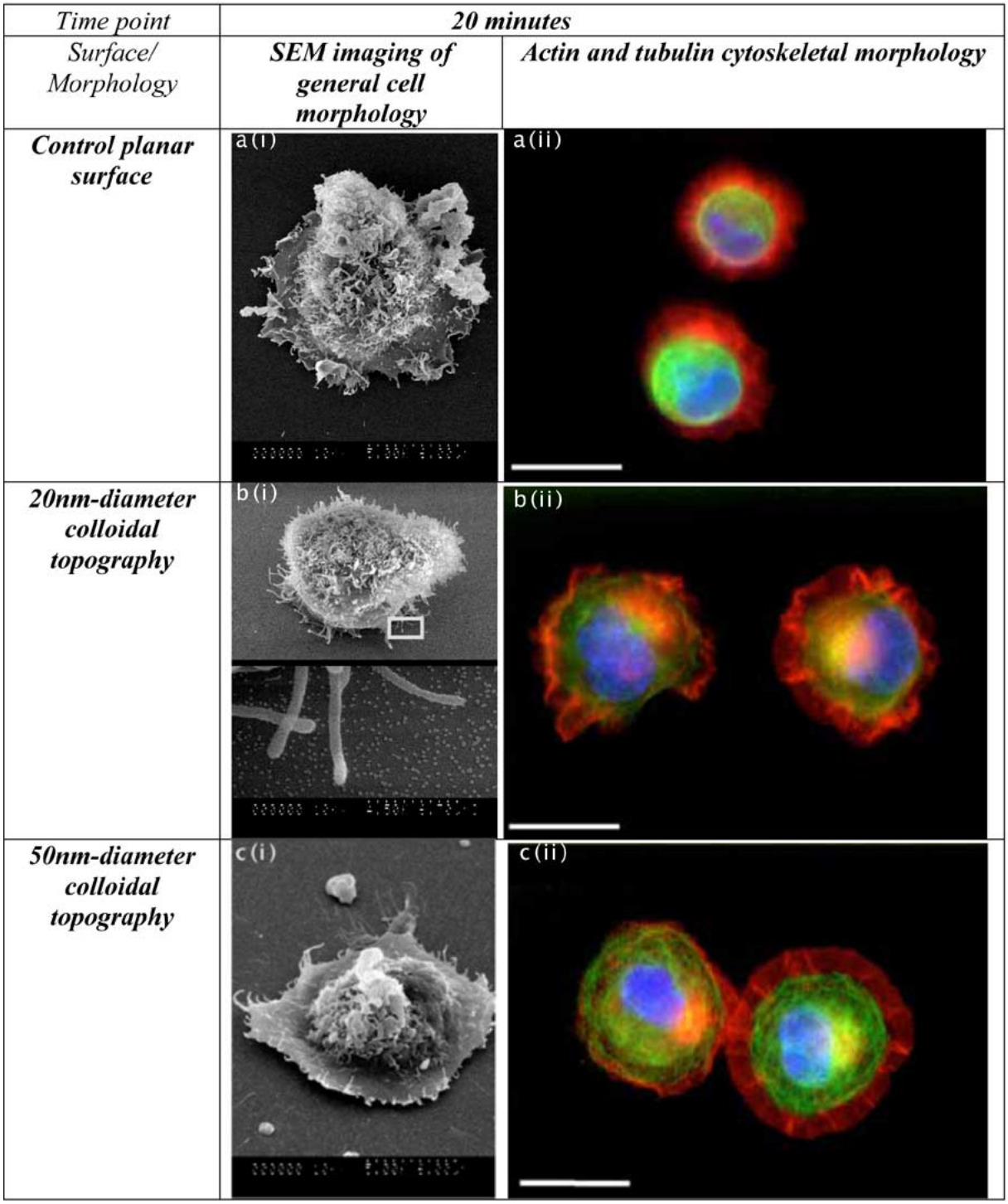

Fig. 2. Fibroblast morphology imaged using FESEM (Hitachi S-900) and fluorescent imaging (Vickers M17 microscope) of the F-actin (red) and tubulin (green) cytoskeleton on planar, 20-, and 50-nm-diameter colloidal nanotopographies at 20 min. Cell nuclei are depicted in blue. Fibroblasts on the planar control appear relatively rounded, a(i), with suggestion of actin development in the form of lamella ruffling and little sign of tubulin network development, a(ii). In contrast, cells on the 50-nm-diameter colloidal topography appear more spread, c(i), with more organized cytoskeletal features, c(ii). Fibroblasts on the 20-nm-diameter colloidal topography are relatively rounded with filopodia extending toward the sample surface supporting the cell above the substrate, b(i). Actin-rich lamella appear less rounded and irregular on the 20-nm-diameter colloids, b(ii), in comparison to features on the planar control and 50-nm-diameter colloidal topography.

and was calculated by constructing a Tukey trellis for two-way ANOVA (Table III).

There are nine sample means whose differences are statistically significant in relation to the 36 calculated, Table III. The mean number of fibroblasts adhering to planar and 20-nm-diameter colloidal substrates at 20 min and planar and 50-nm-diameter colloidal substrates at 20 min are statistically significant, indicating fibroblast adhesion is altered on the colloidal substrates in comparison to planar controls at 20 min. Significant differences were also calculated between the number of cells adhering to the planar substrate at 20 min and: 1) the 20-nm-diameter colloids at 1 h and 2) the 50-nm-diameter colloids at 1 h. These differences highlight alterations in cell response to both colloidal nanotopographies

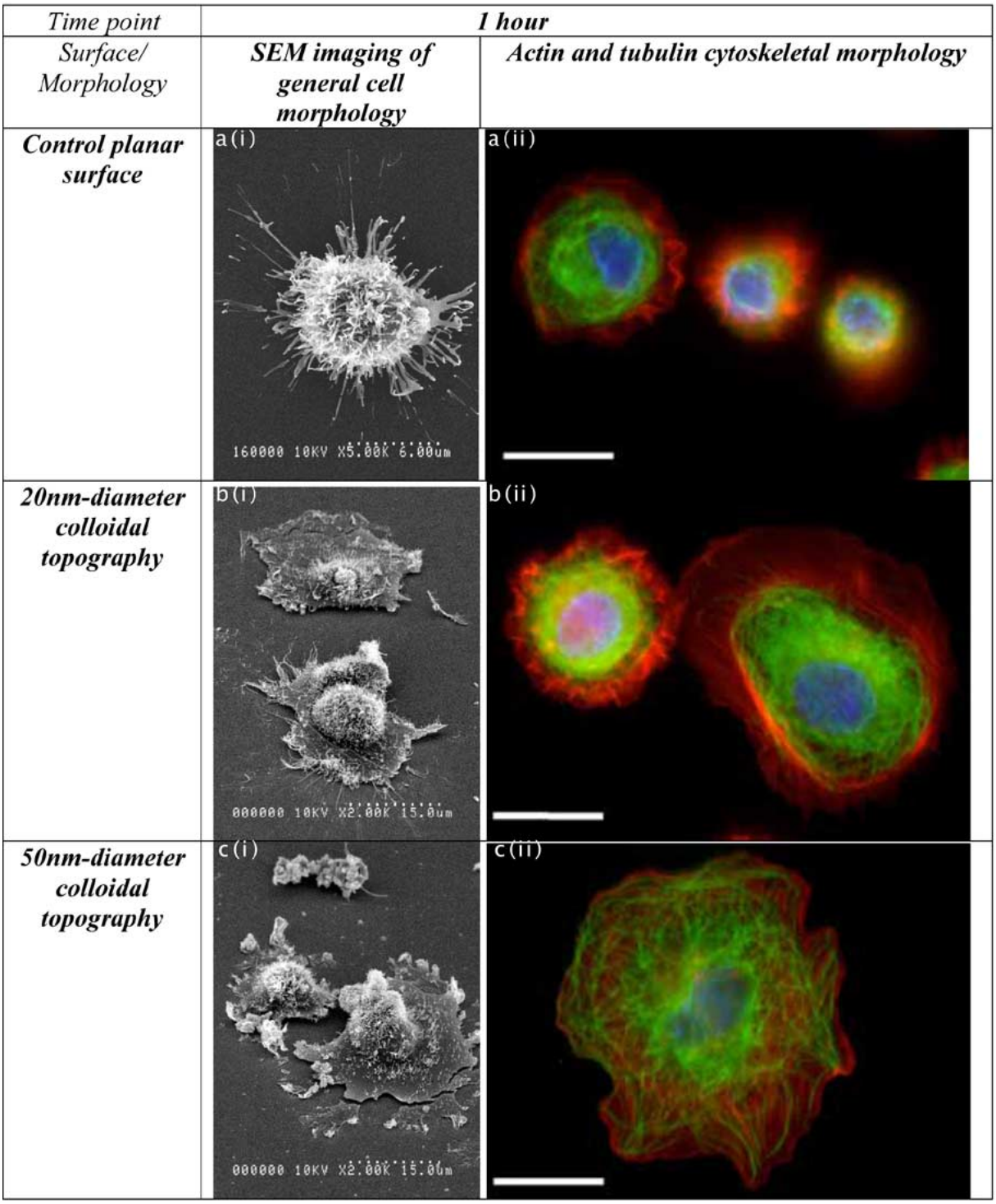

Fig. 3. Fibroblast morphology imaged using FESEM (Hitachi S-900) and fluorescent imaging (Vickers M17) of the F-actin (red) and tubulin (green) cytoskeleton on planar, 20-, and 50-nm-diameter colloidal nanotopographies at 1 h. Nuclei are blue. Fibroblasts on the planar substrate appear relatively rounded, a(i) with actin-rich lamella ruffling, but little sign of tubulin filament formation, a(ii). In contrast, cells on the 20- and 50-nm-diameter colloidal topographies appear much more spread, b(i) and c(i), respectively. Actin appears concentrated toward the cell peripheries on the colloidal topographies, and is particularly prevalent in cells on the 20-nm-diameter colloids, b(ii). Tubulin networks are visible in fibroblasts on the colloidal substrates and are particularly prevalent in cells on the 50-nm-diameter colloids, c(ii).

at 1 h in comparison to the planar control at 20 min. A further significant difference is recorded between the number of cells adhering to 50-nm-diameter colloids at 1 h and planar surface at 3 h, again indicating differences in fibroblast adhesion between experimental and control substrates at different time intervals. Furthermore, significant differences were calculated between fibroblast adhesion on the 20- and 50-nm-diameter colloidal substrates at different times (20-nm-diameter at 20 min and 50-nm-diameter colloids at 3 h, 20-nm-diameter at 1 h and 50-nm-diameter colloids at 3 h and 50-nm-diameter at 1 h and 20-nm-diameter colloids at 3 h). These results suggest that different cell–substrate interactions occur between the

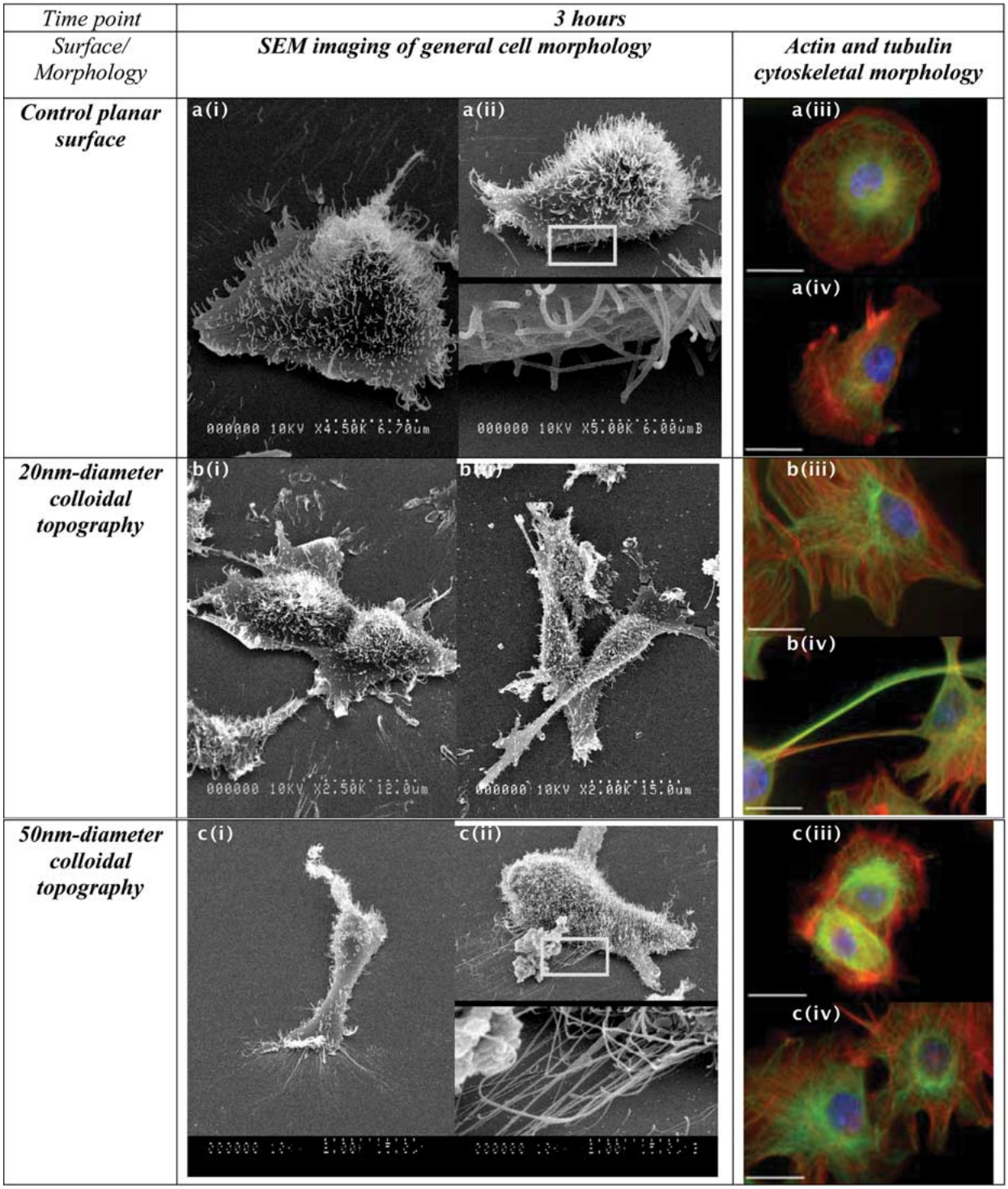

Fig. 4. Fibroblast morphology imaged using FESEM (Hitachi S-900) and fluorescent imaging (Vickers M17 microscope) of the F-actin (red) and tubulin (green) cytoskeleton on planar, 20-, and 50-nm-diameter colloidal nanotopographies at 3 h. Cell nuclei are blue. Cells on the planar substrate appear well spread, but not contacting neighbors, a(i), with filopodia extending toward the sample surface, a(ii). Spread cells exhibit relatively smooth, actin-rich peripheries on the control substrates with defined tubulin networks, a(iii), and morphologies suggest cells are capable of motile behavior, a(iv). Fibroblasts on the 20-nm-diameter colloidal substrate also appear spread, but contact, b(i) and (iii), or overlap, b(ii) and (iv), their neighbors. When cells are in contact with one another on the 20-nm-diameter colloids, it is difficult to differentiate between the surface morphology, b(i), and actin and tubulin cytoskeleton, b(iii), of individual fibroblasts. Elongated membranous features overlapping neighboring cells, b(ii), appear to contain F-actin and are rich in microtubules, b(iv). Similar cell–cell contacts are observed on the 50-nm-diameter colloidal topography, c(iii) and (iv), where cytoskeletal features are merged together between cells, although overlapping of cells is absent. Furthermore, fibroblasts on the 50-nm-diameter colloids extend filopodia across great distances at their leading edges, c(i), and also cascades of extensions at their peripheries, c(ii), which, when cross referenced with the immunohistochemistry images, contain some microtubules and appear actin-rich, c(iii) and (iv).

different nanotopographies at different time points. Interestingly, cell adhesion on the 50-nm-diameter colloids at 1 h and 50-nm-diameter colloids at 3 h are significantly different, indicating the affects of temporal alterations in

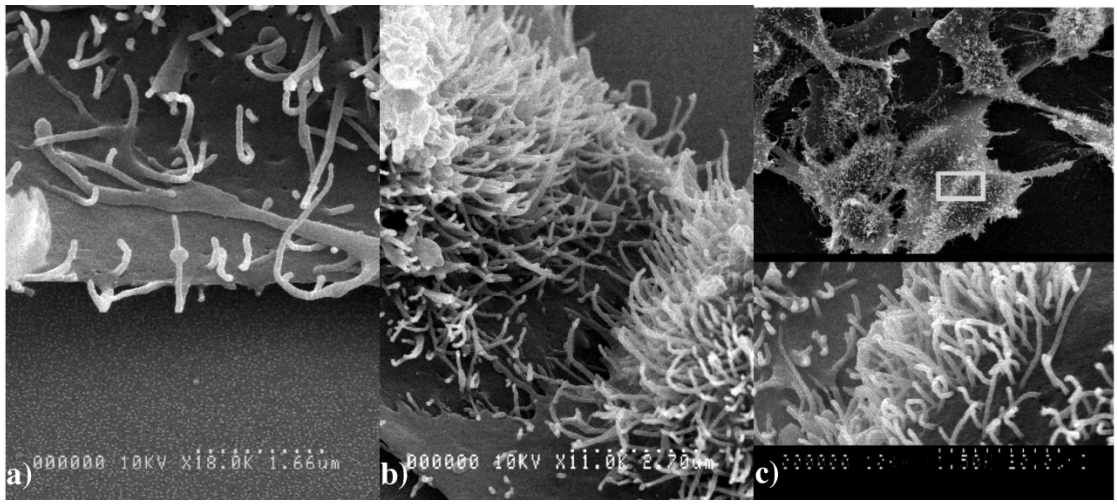

Fig. 5. SEM images of "stickle-bricking" on 20-nm-diameter (a) and (b), and 50-nm-diameter colloidal topographies, where cell–cell contacts between fibroblasts are identified even though areas of the substrate remain unpopulated. Cell–cell contacts generally appear as a result of protrusion entanglement on colloidal substrates, (b) and (c). However, in some instances on the 20-nm-diameter colloids, individual elongations appear to harness one cell to another, (a).

relation to fibroblast adhesion on the 50-nm-diameter colloidal topography.

C. Fibroblast Morphology and Cytoskeletal Organization in Relation to Colloidal Nanotopographies

Immunohistochemistry was utilized to identify filamentous actin and tubulin distribution in relation to fibroblasts on planar, 20-, and 50-nm-diameter colloidal substrates at 20 min, 1 h (Figs. 2 and 3, respectively), and 3 h (Figs. 4 and 5). FESEM was utilized in conjunction with fluorescent imaging to substantiate morphology characteristics as a result of substrate topography and time and also to identify interactions occurring between cells and nanofeatures present within their environment. Following seeding on the substrates, fibroblast morphology was investigated at 20 min (Fig. 2). Cells on the planar surface appeared rounded [Fig. 2(a(i))] with signs of actin-rich lamella formation at their peripheries [Fig. 2(a(ii))]. Similarly, fibroblasts on the 20-nm-diameter colloidal topography appeared rounded; however filopodia appeared in some instances to elevate cells above the nanotopography [Fig. 2(b(i))] and actin located toward the membrane periphery appeared irregularly distributed, deviating from the concentric aspect observed in control cells at this time. In comparison, fibroblasts on the 50-nm-diameter colloidal topography appear well spread [Fig. 2(c(i))], with actin ruffling occurring at cell peripheries and relatively structured microtubule networks [Fig. 2(c(ii))]. At 1 h (Fig. 3), cells on the control surface still appear rounded [Fig. 3(a(i))], with actin-rich ruffles present, but little sign of tubulin network development [Fig. 3(a(ii))]. However, fibroblasts on the colloidal nanotopographies appear more spread [Fig. 3(b(i)) and (c(i))], with actin localized at cell peripheries, particularly prevalent in cells on the 20-nm-diameter colloidal substrate [Fig. 3(b(ii))] and visible tubulin networks, especially in cells on the 50-nm-diameter colloids where microtubules are observed to extend to the very most peripheral regions [Fig. 3(c(ii))]. At 3 h (Fig. 4), cells on the planar substrate appear to have spread out across the surface [Fig. 4(a(i))] and extend filopodia toward the immediate sample surface [Fig. 4(a(ii))] but are not noted to contact neighboring fibroblasts. Actin constitutes the bulk cytoskeletal features present at the peripheral membrane and microtubule networks are also visible in the control fibroblasts [Fig. 4(a(iii))]. Motile behavior is also suggested in cell morphology on the planar substrate [Fig. 4(a(iv))], where a leading edge with actin lamella leads a rear detachment site. Fibroblasts on the 20-nm-diameter colloidal substrate also appear spread, but contact [Fig. 4(b(i)) and (iii)] or overlap [Fig. 4(b(ii)) and (iv)] their neighbors. When cells are in contact with one another on the 20-nm-diameter colloids, it is difficult to differentiate between the surface morphology [Fig. 4(b(i))] and actin and tubulin cytoskeleton [Fig. 4(b(iii))] of individual fibroblasts. Elongated membranous features overlapping neighboring cells [Figs. 4(b(ii)) and 5(a) and (b)] appear to contain F-actin and are rich in microtubules [Fig. 4(b(iv))]. Similar cell–cell contacts are observed on the 50-nm-diameter colloidal topography [Figs. 4(c(iii)), 4(c(iv)), and 5(c)], where cytoskeletal features are merged together between cells, although overlapping of cells is absent. Furthermore, fibroblasts on the 50-nm-diameter colloids extend filopodia across great distances at their leading edges [Fig. 4(c(i))] and also cascades of extensions at their peripheries [Fig. 4(c(ii))] which, when cross referenced with the immunohistochemistry images, contain some microtubules and appear actin-rich [Fig. 4(c(iii)) and (iv)].

D. Discussion

Colloidal lithography techniques can be utilized to fabricate nonregular nanotopographies for biological investigations (Fig. 1), which can be characterized by calculating percentage area coverage and interparticle spacing. Increasing colloidal diameter from 20 to 50 nm results in a 2% increase in area coverage of the base substrate and an approximate doubling (61 nm for 20-nm-diameter to 114 nm for 50-nm-diameter colloids) of mean interparticle spacing (Table I). These results can be explained by classic DLVO theory, where London's attraction forces and Debye length will be altered in response to charge affects occurring as a result of increased colloid

volume [42]–[44]. As colloidal gold particles are quasi-spherical and not identical in size and shape due to the reduction process used in their manufacture [33], charge effects for each individual colloid are different. As submonolayer coverage reaches saturation, these factors contribute to the reduction in sticking probability, preventing further colloids reaching and adhering to the base substrate allowing for irregular distribution of the particles [41]. Electrostatic repulsion occurring between individual quasi-spherical colloids results in the irregular submonolayer patterning observed in nanotopographies fabricated utilizing the inexpensive, reproducible, and accessible technique outlined within this paper (Fig. 1). This is of particular interest when considering the possible role of regularity and symmetry of nanofeatures in eliciting specific cell response, where cell adhesion on regular nanopits is reduced in comparison to planar controls, while cell adhesion on irregular nanopillars is increased in comparison to planar controls [18].

With respect to fibroblast adhesion in relation to the nanotopographies, two-way (ANOVA) indicates cell adhesion is altered as a result of colloidal surface patterning when comparing planar, 20-, and 50-nm-diameter colloidal substrates. The mean number of fibroblasts adhering to each individual surface is also affected by time when comparing cells at 20 min, 1 h, and 3 h. Furthermore, two-way ANOVA revealed that an interactive effect between topography and time acts to influence fibroblast adhesion (Table II) and a Tukey test, utilized to identify specific differences between the mean number of fibroblasts adhering to the substrates at each time point (Table III) further compounds this. Specific differences were identified between the mean number of fibroblasts adhering to planar and 20-nm-diameter colloidal substrates at 20 min and planar and 50-nm-diameter colloidal substrates at 20 min. The residual plot of the data further supported increased fibroblast adhesion on the nanotopographies in comparison to planar substrates at this time (Graph 1).

These adhesion results indicate that different cell–substrate interactions are occurring between the different nanotopographies at different time points. Interestingly, cell adhesion on the 50-nm-diameter colloids at 1 h and 50-nm-diameter colloids at 3 h are significantly different, suggesting temporal alterations may occur between the fibroblasts and the 50-nm-diameter colloidal topography, possibly via alterations in FAC assembly and disassembly [45]. With reference to the residual plot of fibroblast adhesion means (Graph 1), a reduction in cell adhesion is observed on the 50-nm-diameter colloids at 3 h in comparison to 1 h. This may occur as a result of reduced cell–substrate interactions during cell motility [2], [46].

The mean number of cells adhering to the three substrates is greatest on the 20-nm-diameter colloids at 20 min and 50-nm-diameter colloids at 1 h (Graph 1), suggesting similar cellular adhesion mechanisms may act in relation to the nanotopographies. It is interesting to note at the final time point, 3 h, the mean number of fibroblasts adhering to planar, 20-, and 50-nm-diameter colloids is very similar. This observation indicates colloidal topographies are highly adhesive at early times, becoming less adhesive over time. The reduction in adhesion on the experimental substrates results in the mean number of cells adhering to the nanotopographies being similar to that observed on the planar control surface at 3 h suggesting adhesive adaptation of fibroblasts on the colloidal surfaces.

Tubulin and actin cytoskeletal morphology is altered in fibroblasts responding to colloidal topographies (Figs. 2–4). Developed microtubule networks are observed in spread fibroblasts on the nanotopographies at 20 min (Fig. 2), especially in relation to the 20-nm-diameter colloids [Fig. 2(b(ii))], while nonpolarized tubulin is observed in cells on planar controls [Fig. 2(a(ii))]. This is of particular interest when considering cell reactions to microtopography. For example, Wojciak-Stothard and colleagues [12] noted the development of microtubule networks at 30 min on grooved microtopography in comparison to controls and Oakley and Brunnette [13] noted that microtubules were the first cytoskeletal feature to align to the bottom of V-shaped grooves. These observations suggest similar microtubule behavior on both microtopographies and nanotopographies at early times. SEM micrographs indicate fibroblasts exhibit a more spread morphology on 50-nm-diameter colloidal topographies at 20 min in comparison to 20-nm-diameter colloidal and planar control surfaces (Fig. 2). Furthermore, fibroblasts seeded on 20-nm-diameter colloidal topographies extend filopodia at basolateral sites and appear capable of elevating their main bulk above the nanopatterned surface. These protrusions appear to interact with the nanopatterned substrate, functioning as a means of cell–substrate connection. These cell–substrate interactions may account for the increase in fibroblast adhesion on the 20-nm-diameter colloidal substrate at 20 min in comparison to cells on the 50-nm-diameter colloidal and control surfaces.

At 1 h, fibroblasts appear more spread on the colloidal substrates in comparison to the planar controls (Fig. 3). Although well spread on the topographies, SEM images indicate that nuclear regions of the fibroblasts still appear rounded in comparison to the main bulk of the cell body [Fig. 3(b(i)) and (c(i))]. Actin-rich lamellae are present at the peripheries of all fibroblasts; however, microtubule networks appear only in fibroblasts on the colloidal topographies and are extremely well defined in cells on the 50-nm-diameter colloidal substrates [Fig. 3(c(ii))].

Elongated protrusions, observed in fibroblasts on the 20-nm-diameter colloids tend to be mainly composed of microtubule bundles at 3 h [Fig. 4(b(iv))], while on the 50-nm-diameter colloidal topographies at this time [Fig. 4(c(iii)) and (iv)] are composed of spiky actin microfilaments. These features are absent in cells on the control planar substrate [Fig. 4(a(iii)) and (iv))]. Not surprisingly, general fibroblast morphology on the controls and experimental substrates are different, with cells on the 20-nm-diameter colloids appearing most spread and elongated [Fig. 4(b(i)) and (ii)]. Fibroblasts on the 50-nm-diameter colloids also appear elongated in some instances [Fig. 4(c(i))] in comparison to controls [Fig. 4(a(i)) and (ii)]. The increase in defined actin stress fibers over time in hTERT fibroblasts coincides with the development of protrusions, which are observed as an entangled accumulation of these membrane extensions on the 50-nm-diameter colloidal topography at 3 h [Fig. 4(c(ii))]. Fibroblasts on the colloidal topographies have also established cell–cell contacts at 3 h (Fig. 5). "Stickle-bricking," a term used here to describe the entanglement of membrane protrusions at peripheral sites, appears as one possible factor explaining

the observed fibroblast behavior on both 20- [Fig. 5(b)] and 50-nm [Fig. 5(c)] colloidal substrates. However, in some instances on the 20-nm-diameter colloidal topography, cell–cell contacts arise from direct elongated protrusions attaching to neighboring cell membranes, where extensions terminate in prongs [Fig. 5(a)]. Fluorescent imaging of cell–cell contacts at 3 h on the 20-nm-diameter colloidal topography indicates a lack of distinction between actin and tubulin cytoskeletons of fibroblasts that have established contact [Fig. 4(b(iii)) and (b(iv))].

IV. Conclusion

In conclusion, colloidal topographies are observed to alter fibroblast adhesion, morphology, and behavior in relation to control, planar substrates. Furthermore, 20- and 50-nm-diameter colloidal topographies are observed to elicit different responses in hTERT fibroblasts. Both 20- and 50-nm-diameter colloidal topographies result in increased fibroblast adhesion at 20 min and 1 h, however, by 3 h, adhesion is similar to control, planar surfaces. Both tubulin and actin cytoskeletal elements are observed to be involved in these behaviors. At early times of up to 3 h, spread fibroblasts exhibit developed microtubule networks and defined stress fibers on the colloidal substrates. Elongated protrusions appear to be composed mainly of microtubules on the 20-nm-diameter colloidal substrate and microfilaments in the form of microspikes on the 50-nm-diameter colloidal surface at 3 h. Contact inhibition appears altered in fibroblasts on colloidal topographies, as cell–cell contacts are observed in the presence of uninhabited, cell-free surfaces. Elongated membrane protrusions are also observed in these cell types on both the 20- and 50-nm-diameter colloidal topographies. Individual fibroblast boundaries are indistinguishable in intercellular contacts observed on the colloidal topographies. These results indicate cell behavioral alterations in response to colloidal nanotopographies are dependent on feature size. Colloidal diameter also controls feature distribution, indicating feature frequency or pitch within nanopatterned colloidal topographies may contribute to the different cell behaviors observed when comparing fibroblast reactions to both the 20- and 50-nm-diameter colloidal substrates.

These preliminary results indicate that irregular colloidal patterns should not be considered without further study for general implant patterning due to their highly adhesive nature with respect to fibroblasts at early times. Increasing adhesive interactions between fibroblasts and implant materials would be likely to result in fibrous encapsulation of the foreign body, especially if it were mobile [10]. However, colloidal topographies do offer potential applications for topical wound healing, where increased adhesive interactions would prove advantageous with respect to closure of wounds via actin contraction "purse-string" effects, especially with respect to the 50-nm-diameter colloids, or "zippering" effects, where fibroblast protrusions interact with neighboring elongations resulting in cell–cell contact and site closure, specifically in relation to the 20-nm-diameter colloidal substrates [47], [48]. Furthermore, materials enhanced using colloidal-based lithography techniques could be used to produce a substrate attractive to fibroblasts, which may offer a technique of rapid proliferation or granulation resulting in faster wound healing [11].

Acknowledgment

The authors would like to thank Dr. M. Jones, Keele University, Keele, U.K., for her discussion on biostatistics.

References

[1] A. R. Horwitz and J. T. Parsons, "Cell migration—movin' on," *Science*, vol. 286, no. 5442, pp. 1102–1103, 1999.

[2] A. Huttenlocher, M. H. Ginsberg, and A. F. Horwitz, "Modulation of cell migration by integrin-mediated cytoskeletal linkages and ligand-binding affinity," *J. Cell Biol.*, vol. 134, no. 6, pp. 1551–1562, 1996.

[3] D. O. Meredith, G. R. Owen, I. ap Gwyn, and R. G. Richards, "Variation in cell–substratum adhesion in relation to cell-cycle phases," *Exp. Cell Res.*, vol. 293, pp. 58–67, 2004.

[4] B. Geiger and A. Bershadsky, "Assembly and mechanosensory function of focal contacts," *Curr. Opin. Cell Biol.*, vol. 13, no. 5, pp. 584–592, 2001.

[5] A. E. Alpin, A. K. Howe, and R. L. Juliano, "Cell adhesion molecules, signal transduction and cell growth," *Curr. Opin. Cell Biol.*, vol. 11, pp. 737–744, 1999.

[6] G. M. Cooper, *The Cell: A Molecular Approach*, 2nd ed. Sunderland, MA: Sinauer, 1999 [Online]. Available: http://www.ncbi.nlm.nih.gov, at Pubmed

[7] S. M. Schoenwaelder and K. Burridge, "Bidirectional signalling between the cytoskeleton and integrins," *Curr. Opin. Cell Biol.*, vol. 11, pp. 274–286, 1999.

[8] B. Kasemo and J. Gold, "Implant surfaces and interface processes," *Adv. Dental Res.*, vol. 13, pp. 8–20, 1999.

[9] S. Britland, H. Morgan, B. Wojciak-Stodhard, M. Riehle, A. Curtis, and C. Wilkinson, "Synergistic and hierarchical adhesive and topographic guidance of BHK cells," *Exp. Cell Res.*, vol. 228, pp. 313–325, 1996.

[10] J. M. Morehead and G. R. Holt, "Soft-tissue response to synthetic biomaterials," *Otolaryngol. Clin. North Amer.*, vol. 27, pp. 195–201, 1994.

[11] C. F. Koopmann, Jr., "Cutaneous wound healing. An overview," *Otolaryngol. Clin. North Amer.*, vol. 28, pp. 835–845, 1995.

[12] B. Wojciak-Stodhard, A. S. G. Curtis, W. Monaghan, M. McGrath, I. Sommer, and C. D. W. Wilkinson, "Role of the cytoskeleton in the reaction of fibroblasts to multiple grooved substrata," *Cell Motil. Cytoskel.*, pp. 147–158, 1995.

[13] C. Oakley and D. M. Brunette, "The sequence of alignment of microtubules, focal contacts and actin filaments in fibroblasts spread on smooth and grooved titanium substrata," *J. Cell Sci.*, vol. 106, no. 1, pp. 343–354, 1993.

[14] M. Miyaki, K. Fujimoto, and H. Kawaguchi, "Cell response to micropatterned surfaces produced with polymeric microspheres," *Colloids Surf. A, Physiochem. Eng. Aspects*, vol. 153, pp. 603–608, 1999.

[15] H. G. Craighead, C. D. James, and A. M. P. Turner, "Chemical and topographical patterning for directed cell attachment," *Curr. Opin. Solid State Mater. Sci.*, vol. 5, pp. 177–184, 2001.

[16] P. Hanarp, D. Sutherland, J. Gold, and B. Kasemo, "Nanostructured model biomaterial surfaces prepared by colloidal lithography," *Nanostruct. Mater.*, vol. 12, pp. 429–432, 1999.

[17] G. Maheshwari, G. Brown, D. A. Lauffenburger, A. Wells, and L. G. Griffith, "Cell adhesion and motility depend on nanoscale RGD clustering," *J. Cell Sci.*, vol. 113, pp. 1677–1686, 2000.

[18] A. S. G. Curtis, B. Casey, J. O. Gallagher, D. Pasqui, M. A. Wood, and C. D. W. Wilkinson, "Substratum nanotechnology and the adhesion of biological cells. Are symmetry or regularity of nanotopography important?," *Biophysical Chemistry*, vol. 94, pp. 275–283, 2001.

[19] M. A. Wood, D. O. Meredith, and G. R. Owen, "Steps toward a model nanotopography," *IEEE Trans. NanoBiosci.*, vol. 1, no. 4, pp. 133–140, Dec. 2002.

[20] M. A. Wood, M. Riehle, C. D. W. Wilkinson, and Wilkinson, "Patterning colloidal nanotopographies," *Nanotechnology*, vol. 13, pp. 605–609, 2002.

[21] M. J. Dalby, S. J. Yarwood, M. O. Riehle, H. J. H. Johnstone, S. Affrossman, and A. S. G. Curtis, "Increasing fibroblast response to materials using nanotopography: Morphological and genetic measurements of cell response to 13 nm high polymer demixed islands," *Exp. Cell Res.*, vol. 276, pp. 1–9, 2002.

[22] M. J. Dalby, M. O. Riehle, D. S. Sutherland, H. Agheli, and A. S. G. Curtis, "Use of nanotopography to study mechanotransduction in fibroblasts—methods and perspectives," *Eur. J. Cell Biol.*, vol. 83, no. 4, pp. 159–169, 2004.
[23] A.-S. Andersson, F. Bäckhed, A. von Euler, A. Richter-Dahlfors, D. Sutherland, and B. Kasemo, "Nanoscale features influence epithelial cell morphology and cytokine production," *Biomaterials*, vol. 24, pp. 3427–3436, 2003.
[24] R. G. Flemming, C. J. Murphy, G. A. Abrams, S. L. Goodman, and P. F. Nealey, "Effects of synthetic micro- and nano-structured surfaces on cell behavior," *Biomaterials*, vol. 20, pp. 573–588, 1999.
[25] J. Voldman, M. L. Gray, and M. A. Schmidt, "Microfabrication in biology and medicine," *Annu. Rev. Biomed. Eng.*, vol. 1, pp. 401–425, 1999.
[26] M. Riehle, M. Dalby, H. Johnstone, J. O. Gallagher, M. A. Wood, B. Casey, and K. McGhee, "Nanometric surface patterns for tissue engineering: Fabrication and biocompatibility in vitro," in *Proc. Mater. Res. Soc. Symp.*, 2002, vol. 705, pp. Y5.1.1–Y5.1.11.
[27] C. D. W. Wilkinson, M. Riehle, M. A. Wood, J. O. Gallagher, and A. S. G. Curtis, "The use of materials patterned on a nano- and micro-metric scale in cellular engineering," *Mater. Sci. Eng. C*, vol. 19, pp. 263–269, 2002.
[28] A. S. G. Curtis and C. D. W. Wilkinson, "Review: Topographical control of cells," *Biomaterials*, vol. 18, pp. 1573–1583, 1997.
[29] C. D. W. Wilkinson, A. S. G. Curtis, and J. Crossan, "Nanofabrication in cellular engineering," *J. Vac. Sci. Technol. B*, vol. 16, no. 6, pp. 3132–3136, 1998.
[30] P. Clark, P. Connolly, A. S. G. Curtis, J. A. T. Dow, and C. D. W. Wilkinson, "Cell guidance by ultrafine topography in vitro," *J. Cell Sci.*, vol. 99, pp. 73–77, 1991.
[31] S. Turner, L. Kam, M. Isaacson, H. G. Craighead, W. Shain, and J. Turner, "Cell attachment to silicon nanostructures," *J. Vac. Sci. Technol. B*, vol. 15, no. 6, pp. 2848–2854, 1997.
[32] J. O. Gallagher, K. F. McGhee, C. D. W. Wilkinson, and M. O. Riehle, "Interaction of animal cells with ordered nanotopography," *IEEE Trans. NanoBiosci.*, vol. 1, no. 1, pp. 24–28, Mar. 2002.
[33] I. Willner, E. Katz, and A. N. Shipway, "Nanoparticle arrays on surfaces for electronic, optical and sensor applications," *Chemphyschem*, vol. 1, pp. 18–52, 2000.
[34] H. W. Deckman and J. H. Dunsmuir, "Natural lithography," *Appl. Phys. Lett.*, vol. 41, no. 4, pp. 377–379, 1982.
[35] ——, "Applications of surface texture produced with natural lithography," *J. Vac. Sci. Technol. B*, vol. 1, no. 4, pp. 1109–1112, 1983.
[36] T. Sato, Hasko, and H. Ahmed, "Nanoscale colloidal particles: Monolayer organization and patterning," *J. Vac. Sci. Technol. B*, vol. 15, no. 1, pp. 45–48, 1997.
[37] F. Burnmeister, C. Schäfle, T. Mattes, M. Bähmisch, J. Boneberg, and P. Leiderer, "Colloid monolayers as versatile lithographic masks," *Langmuir*, vol. 13, pp. 2983–2987, 1997.
[38] A. S. G. Curtis, "Area and volume measurements by random sampling methods," *Med. Biol. Illus.*, vol. 10, pp. 261–266, 1960.
[39] J. Fowler, L. Cohen, and P. Jarvis, *Practical Statistics for Field Biology*, 2nd ed. Chichester, U.K.: Wiley, 1998.
[40] M. A. Wood, "The application of colloidal nanofabrication to the study of biological systems," Ph.D. dissertation, University of Glasgow, Glasgow, U.K., 2003.
[41] K. C. Grabar, P. C. Smith, M. D. Musick, J. A. Davis, D. G. Walter, M. A. Jackson, A. P. Guthrie, and M. J. Natan, "Kinetic control of interparticle spacing in au colloid-based surfaces: Rational nanometer-scale architecture," *J. Amer. Chemical Society*, vol. 118, pp. 1148–1153, 1996.
[42] R. J. Hunter, *Foundations of Colloidal Science: Volume 1*. Oxford, U.K.: Oxford Sci. Publ., Oxford Univ. Press, 1987.
[43] J. C. Crocker and D. G. Grier, "Interaction and dynamics in charge-stabilized colloids," *MRS Bull.*, vol. 23, pp. 24–31, 1998.
[44] D. Y. C. Chan, "Density functional theory of charged colloidal systems," *Phys. Rev. E*, vol. 63, pp. 061806-1–061806-9, 2001.
[45] S. P. Palecek, A. Huttenlocher, A. F. Horwitz, and D. A. Lauffenburger, "Physical and biochemical regulation of integrin release during rear detachment of migrating cells," *J. Cell Sci.*, vol. 111, pp. 929–940, 1998.
[46] M. Sheetz, D. P. Felsenfeld, and C. G. Galbraith, "Cell migration; regulation of force on extracellular-matrix-integrin complexes," *Trends Cell Biol.*, vol. 8, pp. 51–54, 1998.
[47] K. Woolley and P. Martin, "Conserved mechanisms of repair; from damaged single cells to wounds in multicellular tissues," *BioEssays*, vol. 22, pp. 911–919, 2000.
[48] A. Jacinto, A. Martinez-Arias, and P. Martin, "Mechanisms of epithelial fusion and repair," *Nature Cell Biol.*, vol. 3, pp. E117–E123, 2001.

Mairead A. Wood received the Ph.D. degree from the Centre for Cell Engineering, Glasgow University, Glasgow, U.K., in 2003 under the supervision of Profs. A. Curtis and C. Wilkinson. Her dissertation was entitled "The Application of Colloidal Nanofabrication to the Study of Biological Systems."

She has recently completed a postdoctoral position at the Institute of Science and Technology in Medicine, Keele University, Keele, U.K., investigating dihydropyridine-release strategies to enhance load effects in engineered human bone constructs. She is currently with CCE, University of Glasgow, Glasgow, U.K., working on the EU Framework VI project NANOCUES. Her main research interests lie in the development of cell and tissue engineering strategies for research and clinical applications.

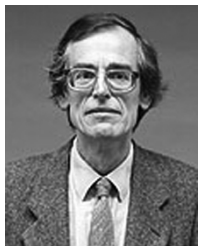

Chris D. W. Wilkinson is the James Watt Professor of Electrical Engineering at the University of Glasgow, Glasgow, U.K. His research embraces or has embraced nanofabrication, waveguides, and reactions of biological cells to micro- and nanostructures. His teaching has ranged over a wide area of electrical engineering from circuits, semiconducting materials, and devices to electromagnetic waves, radar, and electromagnetic computability.

Adam S. G. Curtis is Emeritus Professor of Cell Biology at Glasgow University, Glasgow, U.K. He and Prof. C. Wilkinson founded the Centre for Cell Engineering.